Journal of Materials Chemistry A

Accepted Manuscript

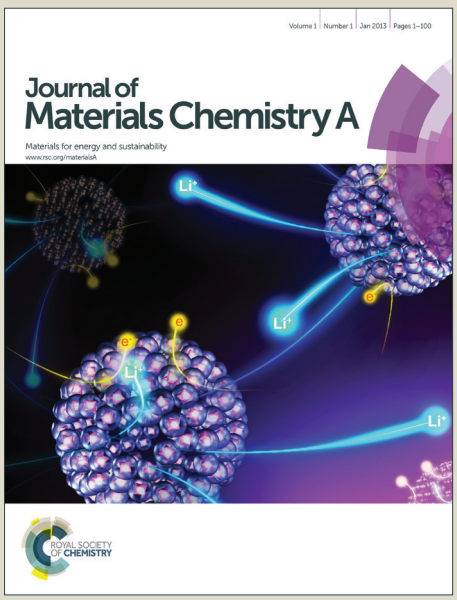

ROYAL SOCIETY OF CHEMISTRY

www.rsc.org/materialsA

Molecular insights into hydrogen bonds in polyurethane/hindered phenol hybrids: evolution and relationship with damping properties

Kangming Xu, Fengshun Zhang, Xianlong Zhang, Qiaoman Hu, Hong Wu*, Shaoyun Guo*

State Key Laboratory of Polymer Materials Engineering, Polymer Research Institute of Sichuan University, Chengdu, Sichuan, 610065, China

ABSTRACT: A polyurethane/hindered phenol system was prepared in the melt in this paper due to keen interests in the still unclear mechanism of hydrogen bonds (H-bonds) in analogous systems. Infrared analysis detected an evolution of intermolecular H-bonds from ester carbonyl/phenolic hydroxyl groups to urethane carbonyl/phenolic hydroxyl groups for the first time. Subsequent dynamic mechanical analysis combined with thermal analysis showed a fluctuation variation of the glass transition temperatures and damping properties of the hybrids. As X-ray diffraction observed the existence of only amorphous hindered phenol in the polyurethane, further molecular dynamic simulation, based on an amorphous cell, characterized the number of H-bonds, the H-bond predominant binding energy and fractional free volume in a quantitative manner. It was observed that the variation tendency of the

* E-mail: wh@scu.edu.cn (Hong Wu); nic7702@scu.edu.cn (Shaoyun Guo).
Tel./Fax: +86-028-85406077 (Hong Wu); +86-028-85405135 (Shaoyun Guo).

simulation data were in accordance with the fluctuation change of the damping properties, thus a relationship was established between the evolution of the H-bonds and the damping properties.

1. INTRODUCTION

Hydrogen bonds (H-bonds), with demonstrated importance in stabilizing static structures and mediating dynamic performances, have attracted enormous attention in recent years.[1-5] They are, for example, the main intermolecular interactions responsible for stabilizing the hybridization of DNA duplexes and holding together the condensed phases of water.[6,7] Moreover, H-bonds also have profound effects on the physical properties of polymer materials. It is found that the destruction of H-bonds network in polyamide-66 greatly influences its glass transition temperature and melting point[8], and the formation of intermolecular H-bonds can enhance the miscibility of polymer blends, such as poly(vinylphenol)/poly(methylmethacrylate)[9] and poly(vinylphenol)/poly(vinylacetate) systems[10], as well as the main concern of this paper: the formation of H-bonds improves the damping properties of polymer mixtures.

Many efforts have been devoted to improving damping properties of polymer mixtures through H-bonds and exploring the mechanisms between them. Wu et al. first introduced hindered phenol into chlorinated polyethylene and attributed the improved damping properties to the dissociation of the intermolecular H-bonds.[11] Meanwhile, by the addition of a tertiary component: chlorinated paraffin into the

above binary system, they believed that the intermolecular H-bonds could be altered, thus the damping property could be regulated.[12] Zhao et al. prepared a nitrile butadiene rubber/hindered phenol hybrid with improved tensile strengths and high damping properties.[13] Moreover, by combining molecular dynamics (MD) simulation, they first explored the H-bond mechanism in a quantitatively manner and attributed the cause of maximum dynamic loss factor to the largest number of H-bonds and the greatest binding energy as well as the minimum fractional free volume.[14] However, due to the versatility of H-bonds in the hybrids, the molecular mechanism for improving damping properties of polymers is still not well established. In particular, the mechanism of H-bonds in polymer with multiple proton acceptors has never been studied. The relationship between microstructure and properties of such systems is also unclear.

In order to characterize structural and spectroscopic properties related to H-bonds, two of the most useful approaches are infrared spectroscopy, in particular, two-dimensional infrared (2D IR) spectroscopy[15-19] and MD simulation.[20, 21] It is widely accepted that the formation of the H-bond X-H---Y results in weakening both the bond of X-H and the bond adjacent to Y, thus leading to the decrease of vibration frequency of X-H and Y species. The decreased frequency can be detected by IR spectroscopy, which provides unambiguous information about the formation of H-bonds. However, in some special cases, certain useful information on H-bonds could not been easily "decoded" from the overlapped conventional IR spectral analysis. 2D IR correlation spectroscopy can extract information that cannot be

obtained straight forwardly from one-dimensional spectroscopy, since the spectral resolution can be enhanced by spreading peaks along the second dimension.[22-25] Therefore, 2D IR correlation spectroscopy has become a powerful and versatile tool for elucidating subtle spectral changes induced by an external perturbation. On the other hand, MD simulation provides one of the most direct ways to theoretically investigate molecular behavior[26], which is not accessible to experimental approaches in complex systems, such as a system involving H-bond interactions.[27] Furthermore, in order to obtain useful insight into the H-bond dynamics, it is important to establish the correlation between the simulation results of structural or vibrational properties and experimental measurement results.[28]

Therefore, in order to investigate the H-bonds in polymers with multiple proton acceptors, thermoplastic polyurethane (TPU), with the potentiality of replacing rubbers in damping fields, is selected as the matrix. It is a block polymer composed of soft segments (SSs) and hard segments (HSs). The SS consists mainly of polyesters or polyethers, while the HS is composed of the diisocyanate component and a low molecular-weight diol. Thus multiple proton acceptors exist in the mainchain. A polyester-based TPU/hindered phenol system is prepared in this paper. By a combination of 2D IR and MD simulation, the purpose is to: (1) investigate the detailed multiple H-bonds behavior in TPU/hindered phenol hybrids at the molecular level and in a quantitative manner and (2) establish the correlation between H-bonds dynamic and damping mechanism of TPU hindered phenol hybrids.

2. EXPERIMENTAL SECTION

2.1. Materials. Polyester-based TPU (Elastollan S70A11), with hardness 70 shore A, density 1.120 g/cm^3 and 4,4'-methane diisocyanate (MDI) within the HSs, were purchased from Elastogran, BASF group (Germany). The hindered phenol triethylene glycol bis(3-tert-butyl-4-hydroxy-5-methylphenyl)propionate (AO-70 or KY-2080), in powder form, was obtained from Beijing Additive Research Institute (Beijing, China). Tetrahydrofuran (analytical grade) was purchased from Chengdu Kelong Chemical Reagent Factory (Chengdu, China). All materials were used without further purification and the molecular structure of TPU and AO-70 are showed in Figure 1.

2.2. Sample preparation. TPU/AO-70 binary hybrids were prepared as follows:

(1) The as-received TPU and AO-70 were dried in a vacuum oven at 80°C and 50°C for 6 h and 24 h, respectively.

(2) The dried TPU was first hot sheared in a Haake internal mixer (Rheocord 90, Germany) at a rotor speed of 30 rpm for 3 min at 185°C.

(3) AO-70 powders with weight ratios of 0phr, 5phr, 15phr, 25phr, 35phr and 45phr were added to the sheared TPU, respectively.

(4) The mixtures were mixed in the Haake internal mixer at a rotor speed of 30 rpm for another 7 min at 185°C to prepare the binary hybrids. These are designated, respectively as TAO-0phr to TAO-45phr.

In order to get mixed samples for characterization, the hybrids were first dried at 80°C for 12 h, then preheated at 185°C for 10 min, hot-pressed at 185°C for 5 min under 12 MPa, and then cool-pressed at room temperature under 12 MPa.

2.3. Characterization.

2.3.1. Fourier Transform Infrared Spectroscopy (FTIR). The temperature-dependent absorbance of FTIR spectra of TPU，AO-70 and the hybrids were recorded with a 4 cm^{-1} spectral resolution on a Nicolet-IS10 (Thermo Electron Co., USA) spectrometer by signal averaging 20 scans. Two pieces of microscope KBr windows, which have no absorption bands in the middle IR region, were used to prepare a transmission cell. Variable-temperature spectra, controlled by a temperature control instrument including a programmed heating cell and a circulating water jacket cooling system, were collected between 25 and 210°C with increments of 5°C. All samples were prepared via solvent casting from 1 g/L tetrahydrofuran solution, dried in a vacuum oven at 80°C for 12 h and protected by dried high-purity nitrogen gas during the measurement. The baseline correct processing was performed by the automatic baseline correction of OMNIC 8.2 spectral collecting software (Thermo Fisher Scientific Inc., USA).

2.3.2. Two-Dimensional (2D) Correlation Analysis. Spectra recorded at an interval of approximately 10°C were selected in certain wavenumber ranges and the generalized 2D correlation analysis was applied by the 2D Shige software composed by Shigeaki Morita (Kwansei-Gakuin University, Japan). In the 2D correlation maps,

the red regions (red peaks in the maps) are defined as the positive correlation intensities, whereas the blue regions (blue peaks in the maps) are regarded as the negative correlation intensities.

2.3.3. Dynamic mechanical analysis (DMA). Dynamic mechanical spectra were acquired through a dynamic mechanical analyzer (Q800, TA Instrument). The samples with sizes of 10 mm (length) × 10 mm (width) × 1 mm (thickness) were heated from -60 to 120°C at a constant frequency of 10 Hz and a heating rate of 3 ℃ /min under a double-cantilever mode.

2.3.4. Differential scanning calorimetry (DSC). The thermal properties of TPU, AO-70, and the hybrids (5–7 mg) were measured using differential scanning calorimetry (Q20, TA Instrument). The Nitrogen gas was purged throughout the measurements. The sample was first heated from room temperature to 210°C (first heating) to eliminate heat history. Subsequently, the sample was cooled to -80°C and heated again to 210°C (second heating). All the heating and cooling rates were 10 °C/min. The glass transition temperature (Tg) were obtained from the second heating scan. The melting temperature (Tm) of the as-received AO-70 was obtained from the first heating scan.

2.3.5. Wide-angle X-ray diffraction (WXRD). WXRD measurements were performed on an X'Pert Pro X-ray diffractometer (Philips) using Cu Kα radiation (λ = 0.154 nm, 40 kV, 40 mA) at room temperature. The scanning rate was 8 °/min.

2.4. Simulation Strategies for TPU/AO-70 hybrids. MD simulation had been

performed on the TPU/AO-70 hybrids at ambient temperature (25°C) using the software packages of Discover and Amorphous cell modules (Accelrys, Inc., San Diego, CA) with the Material Studio Modeling (version 5.0). The COMPASS (condensed-phase optimized molecular potentials for atomistic simulation studies) force field was used for computing interatomic interactions.[29] This force field had been widely used to optimize and predict the structural, conformational, and thermophysical condensed phase properties of polymers. In the COMPASS force field approach, total energy, E_T of the system was represented by the sum of bonding and nonbonding interactions given as the following:

$$E_T=E_b+E_o+E_\varphi+E_{loop}+E_{pe}+E_{vdw}+E_q \quad (1)$$

Here, the first five terms represent the bonded interactions, which correspond to energies associated with the bond, E_b; bond angle bending, E_o; torsion angle rotations, E_φ; out of loop, E_{loop}; and potential energy, E_{pe}. The last two terms represent nonbonded interactions, which consist of van der Waals term, E_{vdw}, and electrostatic force, E_q.[30] Initial velocities were set by using the Maxwell-Boltzmann profiles at 25°C. The verlet velocity time integration method was used with the time step of 1 femtosecond (fs).[31]

The chemical structure of TPU was exhibited in Figure 1(b), where R and R' represented the HSs and the SSs, respectively. This practical structure of TPU performed in experiment displayed a linear structure with stiff chains as well as soft chains coexisted that made simulation difficult to perform. Therefore, a predigested

method, which simplified the structures of HSs and SSs, was used to construct the TPU structure in this paper. To build the model of TPU, R was set to be

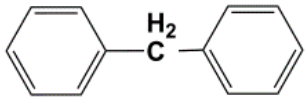

and R' to be

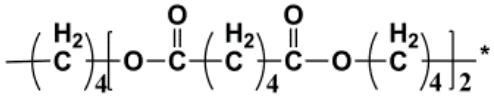

based on the practical structure of polymer used in the experiment, and five degrees of polymerization were adopted.[32] To choose TPU chain length for MD simulation, individual TPUs were first subjected to minimization and then dynamics was performed to find the solubility parameter, which was plotted vs the number of repeating units of TPU as Figure 2 showed. When a stable value was obtained, it confirmed that the number of repeating units was sufficient for simulation. In the present work, TPU consisting of 18 repeating units had been adopted.

Figure 3 shows the process of MD simulation. After the construction of the amorphous cell with a periodic boundary (Figure 3(a)-(c)), the cell was energy minimized with the steepest descent method and the conjugate gradient method. Subsequently, in order to adjust the periodic box size and to obtain an energy equilibrated cell, the cell was equilibrated in the isothermal-isobaric (NPT) ensemble at 1 atm and 25°C. This equilibration was done for 1 nanosecond (ns) with the dynamics that was followed by the data accumulation running for another 1 ns and the

configurations saved for every 5 picosecond (ps) (Figure 3(d)). Finally, the cell could be used to count the number of H-bonds (Figure 3(e)) and to analyze the fractional free volume (FFV) (Figure 3(f)) as well as the binding energy. The FFV of the equilibrated hybrids was determined by a grid scanning method.

3. RESULTS AND DISCUSSION.

3.1. Hydrogen bonds in TAO hybrids. Related to the chemical structure of TPU and AO-70 shown in Figure 1, multiple H-bonds might be formed between two types of proton donators (urethane N-H (Figure 1(8)(9)) and phenolic O-H groups (Figure 1(1)(2))) and three types of proton acceptors (urethane C=O (Figure 1(6)(7)), ester C=O groups in both TPU (Figure 1(5)) and AO-70 (Figure 1(3)(4))) in TAO hybrids. In order to extract the existence of the aforementioned H-bonds, temperature-dependent IR of AO-70, TAO-0phr and TAO-45phr in the O-H, N-H and C=O group regions were characterized and the results were shown in Figure 4.

It was well accepted that temperature played an important role in determining the extent of H-bonds. In general, the strength of H-bonds decreased with temperature increasing, resulting in the decreased intensity and the increased wavenumber of H-bonded IR peaks. For pure AO-70 (Figure 4(a)), the peak at 3480 cm^{-1} decreased and shifted to higher wavenumber while a new peak at 3590 cm^{-1} stood out with temperature increasing, which could be attributed to the vibration of H-bonded O-H and free O-H, respectively. Meanwhile, a distinct peak at 1735 cm^{-1} and a latent shoulder peak at 1710 cm^{-1} both decreased and shifted to higher wavenumber with

temperature increasing, which were corresponding to the vibration of free C=O and H-bonded C=O, respectively. Therefore, the H-bonded phenolic O-H/ester C=O were shown to exist in AO-70. However, for TAO-0phr, although the decreased peak at 3332 cm^{-1} and the increased peak at 3390 cm^{-1}, corresponding to the vibration of H-bonded N-H and free N-H, respectively, could be obviously detected, the situation in the C=O region was complex and the multiple latent peaks could not be easily distinguished as Figure 4(b) showed.[33] And TAO-45phr (Figure 4(c)) showed a similar scene as TAO-0phr, except for the arise of the two O-H peaks by the addition of AO-70. Therefore, in order to check out the latent peaks in C=O region and make clear H-bond relationship of TAO hybrids, 2D IR, with higher sensitivity, was applied. And the results were shown below. The results for AO-70 and TAO-15phr were also taken into account for a comparison.

2D IR correlation spectra were characterized by two independent wavenumber axes (x, y) and a correlation intensity axis. Two types of spectra, 2D synchronous and asynchronous spectrum, were obtained in general. In the synchronous spectra, diagonal peaks were referred to as autopeaks. They represented the overall extent of the temperature-induced fluctuation of spectral intensity with respect to the reference spectrum. The off-diagonal peaks were called crosspeaks and their presence indicated that simultaneous changes occurred at two different wavenumbers. Positive crosspeaks (red color) demonstrates the intensity variations of the two peaks at x and y were taking place in the same direction (both increase or both decrease) under the environmental perturbation; while the negative cross-peaks (blue color) helped to

infer that the intensities of the two peaks at x and y change in opposite directions (one increases, while the other one decreases) under perturbation. The asynchronous spectra had only off-diagonal peaks. The intensity of the asynchronous spectrum represented sequential or successive changes of spectral intensities observed at x and y. And this feature was very useful in differentiating overlapped bands due to different spectral origin.[22]

The synchronous and asynchronous maps for the heating process of AO-70 in the 3700-3200 cm^{-1} and 1780-1660 cm^{-1} region are shown in Figure 5. In the synchronous map of 3700-3200 cm^{-1} (Figure 5(a)), two strong autopeaks developed at 3590 and 3480 cm^{-1}, indicating the prominent changes of free and H-bonded O-H with temperature elevating. The negative crosspeaks showed that the heating induced intensity variations of the peaks at 3590 and 3480 cm^{-1} were simultaneously changed in an opposite direction. In the asynchronous map of 3700-3200 cm^{-1} (Figure 5(b)), the crosspeak implied that out-of phase spectral changes occurred at 3590 and 3480 cm^{-1}. The synchronous spectrum (Figure 5(c)) in the 1780-1660 cm^{-1} range was dominated by only one strong autopeak at 1735 cm^{-1}, which was attributed to the vibration of free C=O with temperature elevating. According to the crosspeaks in the asynchronous map of 1780-1660 cm^{-1} (Figure 5(d)), the existence of the peak at 1710 cm^{-1}, attributed to the vibration of H-bonded C=O, could be detected. Therefore, it was confirmed that the results of the above 2D IR analysis were well consistent with that of the temperature-dependent FTIR.

2D IR synchronous and asynchronous maps of TAO-0phr in the 3700–3200 and 1780–1660 cm^{-1} regions are depicted in Figure 6. In the synchronous maps (Figure 6(a),(c)), four autopeaks developed at 3332, 1735, 1705 and 1685 cm^{-1}, indicating the prominent changes of them with temperature elevating. In the asynchronous map of N-H group region (Figure 6(b)), the presence of two symmetrical crosspeaks confirmed the presence of free and H-bonded N-H groups at 3390 and 3332 cm^{-1}, respectively. In the asynchronous map of C=O group region (Figure 6(d)), the presence of five bands (1735, 1721, 1705, 1685 and 1695 cm^{-1}) could be distinguished, which were assigned to the vibration of free C=O group, the H-bonded ester C=O group, the H-bonded urethane C=O group in disordered regions, the H-bonded urethane C=O group in ordered or crystalline regions and the H-bonded urethane C=O group in slightly disordered regions, respectively.[34,35] Therefore, it could be concluded that one kind of ester C=O---N-H H-bond and three kinds of urethane C=O---N-H H-bonds were co-existed in TAO-0phr, i.e. pure TPU.

Figure 7 depicts 2D IR synchronous and asynchronous maps of TAO-15phr in the 3700-3200 and 1780-1660 cm^{-1} region. With adding 15phr AO-70 into TPU, in the asynchronous map of O-H and N-H regions (Figure 7(b)), the presence of the crosspeaks confirmed the existence of free and H-bonded O-H and N-H groups at 3590, 3480, 3390 and 3332 cm^{-1}, respectively. Meanwhile, the existence of six bands (1735, 1725, 1721, 1705, 1695 and 1685 cm^{-1}) could be distinguished in the asynchronous map of C=O region (Figure 7(d)). Compared with that of pure AO-70 and TPU, the new 1725 cm^{-1} band should be attributed to the intermolecular H-bond

between ester C=O group in TPU and phenolic O-H group in AO-70. And the absence of 1710 cm^{-1} band indicated the absence of intramolecular H-bond of AO-70 in TAO-15phr.

Figure 8 depicts 2D IR synchronous and asynchronous maps of TAO-45phr. With adding more AO-70 into TPU, the asynchronous map of O-H region (Figure 8(b)) extracted similar information to that of TAO-15phr whereas in the asynchronous C=O region (Figure 8(d)), an unexpected new band at 1690 cm^{-1} could be distinguished compared with that of TAO-15phr. To our surprise, this band had never been detected before.[36]

To figure out the attribution of the band at 1690 cm^{-1}, 2D IR correlation spectra of TAO-45phr between C=O and H-bonded O-H was compared and the results were shown in Figure 9. In both the synchronous and asynchronous maps, the band at 1725 and 1690 cm^{-1} correlating with the band at 3480 cm^{-1} could be observed, indicating the presence of H-bonds between ester and urethane C=O in TPU with phenolic O-H in AO-70, respectively. And the absence of the 1710 cm^{-1} band also indicates the absence of intramolecular H-bonds of AO-70 in TAO-45phr. Therefore, it could be concluded that the intermolecular H-bonds between AO-70 and SSs of TPU evolved to HSs of TPU and formed an H-bond network with the amount of AO-70 increasing.

3.2. Dynamic mechanical analysis. As mentioned above, H-bonds played a critical role in hybrids containing hindered phenol. To explore the effect of H-bonds evolution on the damping properties of TAO hybrids, the temperature dependence of

the loss factor (tanδ) and the storage module of the hybrids were depicted and the results were shown in Figure 10. From the DMA results, tanδ reflected the internal and external friction and expressed the ratio of dissipated energy in one deformation cycle to energy accumulated during the deformation process. A high value of tanδ mean good damping properties of the material. And the storage modulus was a measure of the capability of a material to store mechanical energy and resist deformation. In Figure 10(a), only one tanδ peak, corresponding to the Tg of SSs of TPU, was detected in all TAO hybrids. Meanwhile, except for TAO-35phr, the value of the peak exhibited a gradually improvement from 0.79 up to 1.10 as well as the position showed a temperature drift from -9.5 to 2.1°C with increasing the amount of AO-70 from 0 to 45phr, indicating an improvement of damping properties in these hybrids. However, a value loss of tanδ and drift of peak toward to low temperature were observed in TAO-35phr, indicating the decline of damping properties in the sample. Moreover, the storage modulus curves showed a similar variation trend with the tanδ curves as shown in Figure 10(b). So it was reasonably concluded that the H-bonds evolution should be the main cause of a fluctuation variation of damping properties in TAO hybrids.

3.3. Compatibility and microstructure. To further confirm the Tg variation observed above and the compatibility in the hybrids, the DSC traces of AO-70 and TAO hybrids were obtained and the results are shown in Figure 11. The as-received AO-70 powder was one kind of crystalline small molecules whose melting temperature was at around 82°C. After the heating to 210°C and quenching to -80°C

with a rate of 10 °C/min, amorphous AO-70 with a Tg at around 7°C was obtained (Figure 11(a)). In TAO hybrids (Figure 11(b)), the shift of the only Tg, attributed to the Tg of the SSs of TPU, showed a similar variation trend with that of DMA results, providing another indication of the fluctuation variation of Tg. Moreover, neither the melting peak nor glass transition peak of AO-70 was observed in the hybrids, indicating that AO-70 was miscible with TPU in all hybrids.

Figure 12 shows the XRD traces of AO-70 and TAO hybrids. The as-received and amorphous AO-70 exhibited typical crystalline and amorphous characteristics, respectively. For TAO hybrids, an only 2θ at about 21^{o}, corresponding to the slight long distance order of TPU, could be observed. Moreover, no crystalline features were detected in all hybrids, suggesting the existence of only amorphous AO-70 in TAO hybrids.

3.4. Analysis of H-bonds in TAO hybrids by MD simulation. Because only amorphous hindered phenol existed in TPU, MD simulation based on an amorphous cell was used to obtain detailed quantitative information about H-bonds in TAO hybrids. The simulation results of the pair correlation function, the number of H-bonds as well as the H-bond predominant binding energy and FFV in the optimized amorphous cell are shown below.

The pair correlation function g(r), related to the probability of finding another atom at a distance r from a specific atom, had been widely applied in studying H-bonds. The distances between atoms of 2.6-3.1, 3.1-5.0, and above 5.0 Å belonged to

H-bonds, strong Van der Waals force, and weak Van der Waals force, respectively.[37] Figure 13 presents the pair correlation function results of intermolecular H and O atoms in the optimized amorphous cell of TAO-25phr. The maximum peaks of the correlation function of H and O lie in 2-3.2 Å, suggesting high probability for the two atoms to form H-bond interaction.

Table 1. Average number of H-bonds in different TAO hybrids by MD simulation

Sample name	The number of O-H/ester C=O of TPU intermolecular hydrogen bonds (H-bonds (a))	The number of O-H/urethane C=O of TPU intermolecular hydrogen bonds (H-bonds (b))	The number of O-H/ester C=O of AO-70 intramolecular hydrogen bonds (H-bonds (c))
TAO-5phr	1	0	0
TAO-15phr	2	0	0
TAO-25phr	3	0	0
TAO-35phr	1	2	0
TAO-45phr	3	1	0

Table 1 lists the average number of different kinds of H-bonds in different TAO hybrids. Five repeated cells obtained by the repeated MD simulation condition were used to obtain the number of H-bonds, and then the average number of H-bonds in different hybrids was obtained. Except for TAO-35phr, with the amount of AO-70 increased from 0 to 45phr, the number of H-bonds (a) gradually increased and reached maximum value in both TAO-25phr and TAO-45phr, meanwhile H-bonds (b)

were only detected in TAO-45phr, which were in accord with the 2D IR results. However, for TAO-35phr the number of H-bonds (a) showed dramatic decrease while that of H-bonds (b) exhibited a maximum value compared with that of TAO-25phr and TAO-45phr, indicating the most dramatic variation of intermolecular H-bonds from SSs to HSs of TPU in TAO-35phr. In addition, no intramolecular H-bonds of AO-70 were detected in all hybrids.

The binding energy ($E_{binding}$), which was defined as the negative of the intermolecular interaction energy (E_{inter}) between two components, could reflect how well two components mix with each other.[38] And, E_{inter} could be evaluated by the total energy (E_{total}) of the mixture and those of the individual components in the equilibrium state. Thus, the $E_{binding}$ between AO-70 and TPU could be determined as follows:

$$E_{binding}=-E_{inter}=-(E_{total}-E_{AO-70}-E_{TPU}) \quad (2)$$

where E_{total}, E_{AO-70} and E_{TPU} are the total energy of the TAO hybrid, AO-70 and TPU, respectively. E_{TPU} is a constant (-2927.42 kcal/mol) because the number of TPU chains were fixed in the amorphous cell.

Table 2. Binding energies of TAO hybrids with different AO-70 amounts.

Sample name	E_{total} (Kcal/mol)	E_{AO-70} (Kcal/mol)	$E_{binding}$ (Kcal/mol)
TAO-5 phr	**-3168.06**	**-149.99**	**90.65**
TAO-15 phr	**-3275.16**	**-243.59**	**104.15**
TAO-25 phr	**-3552.03**	**-507.44**	**117.17**
TAO-35 phr	**-3609.86**	**-653.19**	**29.25**
TAO-45 phr	**-3894.26**	**-888.50**	**78.34**

Table 2 displays the binding energies of TAO hybrids with different AO-70 amounts. Negative E_{total} values indicated that the TAO hybrids were stable. With AO-70 increasing from 0 to 25phr, the binding energy increased to a maximum value, followed by a large decrease to a minimum value in TAO-35phr and a second increase in TAO-45phr, indicating the worst mix between AO-70 and TPU in TAO-35phr because of the variation of H-bonds. Moreover, H-bonds between AO-70 and SSs of TPU were more stable than that with HSs.

According to the Williams-Landel-Ferry (WLF) equation based on the free volume theory[39], FFV, which was commonly used to characterize the efficiency of chain packing and the amount of free space in a polymer matrix, was greatly affected by H-bonds. A common definition of FFV was:

$$FFV = \frac{V - V^*}{V} \tag{3}$$

where V and V^* were the specific volume and occupied volume, respectively. Figure 14 depicted the FFV results of TAO hybrids calculated by MD simulation. With increasing the amount of AO-70, the FFV decreased first and reached a minimum value at TAO-25phr because of the increased amount of H-bonds between AO-70 and SSs of TPU, and then a great increase occurred at TAO-35phr and TAO-45phr, which was attributed to the great variation of H-bonds.

Therefore, combined with the experiment and MD simulation, the structural schematic diagram of TAO hybrids were put forward and shown in Figure 15. Pure

TPU was a block copolymer with SSs and HSs coexisted in the main chain (Figure 15(a)). With AO-70 adding into TPU, it was more likely to be wrapped within SSs to form intermolecular H-bonds (Figure 15(b)). And the larger amount of AO-70, the larger number of the H-bonds, resulting in the increase of the binding energy, the decrease of FFV as well as the improvement of damping properties. However, when a critical amount of AO-70 reached (Figure 15(c)), the SSs were not able to wrap AO-70 at all, thus a variation of intermolecular H-bonds from SSs to HSs of TPU occurred, inducing the minimum value of the binding energy and almost maximum value of FFV, which leaded to the dramatic decrease of damping properties. With more AO-70 existing in TPU (Figure 15(d)), the new formation of large amounts of H-bonds with SSs and the formation of the H-bond network were the main cause of the second improvement of damping properties.

4. CONCLUSIONS.

To conclude, by a combination of MD simulation with experimental analysis including FTIR, especially 2D IR, DMA, DSC and WXRD, the evolution of H-bonds and its relationship with damping properties in TAO hybrids were stated in details. 2D IR observed the existence of AO-70 intermolecular H-bonds both in SSs and HSs of TPU for the first time. The intermolecular H-bonds between AO-70 and SSs of TPU combined with its predominant binding energy and FFV were the main attribution to the improvement of damping properties. And the evolution of H-bonds from SSs to HSs of TPU was the main cause of the declined damping properties.

These fundamental studies are expected to provide some useful information to design and fabricate the high-performance polymeric damping materials.

ACKNOWLEDGEMENTS

Financial supports of the National Natural Science Foundation of China (51273132, 51227802 and 51121001), Program for New Century Excellent Talents in University (NCET-13-0392) and Program for Changjiang Scholars and Innovative Research Team in University (IRT1163) are gratefully acknowledged.

REFERENCES

(1) M. Cowan, B. D. Bruner, N. Huse, J. Dwyer, B. Chugh, E. Nibbering, T. Elsaesser and R. Miller, *Nature*, 2005, **434**, 199-202.

(2) C. Kolano, J. Helbing, M. Kozinski, W. Sander and P. Hamm, *Nature*, 2006, **444**, 469-472.

(3) S. Kitagawa and K. Uemura, *Chemical Society Reviews*, 2005, **34**, 109-119.

(4) I. Benjamin, *The Journal of Physical Chemistry B*, 2005, **109**, 13711-13715.

(5) D. J. Wolstenholme and T. S. Cameron, *The Journal of Physical Chemistry A*, 2006, **110**, 8970-8978.

(6) J. Watson and F. Crick, *Nature*, 1953, **171**, 964.

(7) C. Fecko, J. Eaves, J. Loparo, A. Tokmakoff and P. Geissler, *Science*, 2003, **301**, 1698-1702.

(8) H. A. Karimi-Varzaneh, P. Carbone and F. Muller-Plathe, *Macromolecules*, 2008, **41**, 7211-7218.

(9) J. Dong and Y. Ozaki, *Macromolecules*, 1997, **30**, 286-292.

(10) S. Zhang, P. C. Painter and J. Runt, *Macromolecules*, 2002, **35**, 8478-8487.

(11) C. Wu, T. A. Yamagishi, Y. Nakamoto, S. Ishida, K. H. Nitta and S. Kubota, *Journal of Polymer Science Part B: Polymer Physics*, 2000, **38**, 2285-2295.

(12) C. Wu, *Journal of Polymer Science Part B: Polymer Physics*, 2001, **39**, 23-31.

(13) X.-Y. Zhao, P. Xiang, M. Tian, H. Fong, R. Jin and L.-Q. Zhang, *Polymer*, 2007, **48**, 6056-6063.

(14) B. Qiao, X. Zhao, D. Yue, L. Zhang and S. Wu, *Journal of Materials Chemistry*, 2012, **22**, 12339-12348.

(15) M. Cho, *Chemical reviews*, 2008, **108**, 1331-1418.

(16) S. Woutersen and P. Hamm, *Journal of Physics: Condensed Matter*, 2002, **14**, R1035-R1062.

(17) M. Fayer, *Annual review of physical chemistry*, 2009, **60**, 21-38.

(18) Y. S. Kim and R. M. Hochstrasser, *The Journal of Physical Chemistry B*, 2009, **113**, 8231-8251.

(19) W. Zhuang, T. Hayashi and S. Mukamel, *Angewandte Chemie International Edition*, 2009, **48**, 3750-3781.

(20) Y. Tamai, H. Tanaka and K. Nakanishi, *Macromolecules*, 1996, **29**, 6750-6760.

(21) Y. Tamai, H. Tanaka and K. Nakanishi, *Macromolecules*, 1996, **29**, 6761-6769.

(22) I. Noda, A. Dowrey, C. Marcott, G. Story and Y. Ozaki, *Appl. Spectrosc*, 2000, **54**, 236A-248A.

(23) I. Noda, *Vibrational spectroscopy*, 2004, **36**, 143-165.

(24) Y. Wu, J.-H. Jiang and Y. Ozaki, *The Journal of Physical Chemistry A*, 2002, **106**, 2422-2429.

(25) T. Amari and Y. Ozaki, *Macromolecules*, 2002, **35**, 8020-8028.

(26) O. Alexiadis and V. G. Mavrantzas, *Macromolecules*, 2013, **46**, 2450-2467.

(27) J. Huang, D. Haussinger, U. Gellrich, W. Seiche, B. Breit and M. Meuwly, *The Journal of Physical Chemistry B*, 2012, **116**, 14406-14415.

(28) M. Pagliai, F. Muniz-Miranda, G. Cardini, R. Righini and V. Schettino, *The Journal of Physical Chemistry Letters*, 2010, **1**, 2951-2955.

(29) H. Sun, *The Journal of Physical Chemistry B*, 1998, **102**, 7338-7364.

(30) S. Zhu, L. Yan, D. Zhang and Q. Feng, *Polymer*, 2011, **52**, 881-892.

(31) M. Khalili, A. Liwo, A. Jagielska and H. A. Scheraga, *The Journal of Physical Chemistry B*, 2005, **109**, 13798-13810.

(32) X. Ma, X. Qu, Q. Zhang and F. Chen, *Polymer*, 2008, **49**, 3590-3600.

(33) J. Mattia and P. Painter, *Macromolecules*, 2007, **40**, 1546-1554.

(34) L.-S. Teo, C.-Y. Chen and J.-F. Kuo, *Macromolecules*, 1997, **30**, 1793-1799.

(35) V. G. Gregoriou, S. E. Rodman, B. R. Nair and P. T. Hammond, *The Journal of Physical Chemistry B*, 2002, **106**, 11108-11113.

(36) D. Xiao, X. Zhao, Y. Feng, P. Xiang, L. Zhang and W. Wang, *Journal of Applied Polymer Science*, 2010, **116**, 2143-2150.

(37) X. Ma, W. Zhu, J. Xiao and H. Xiao, *Journal of hazardous materials*, 2008, **156**, 201-207.

(38) M. Solimannejad and I. Alkorta, *The Journal of Physical Chemistry A*, 2006, **110**, 10817-10821.

(39) C. Wu, *Polymer*, 2010, **51**, 4452-4460.

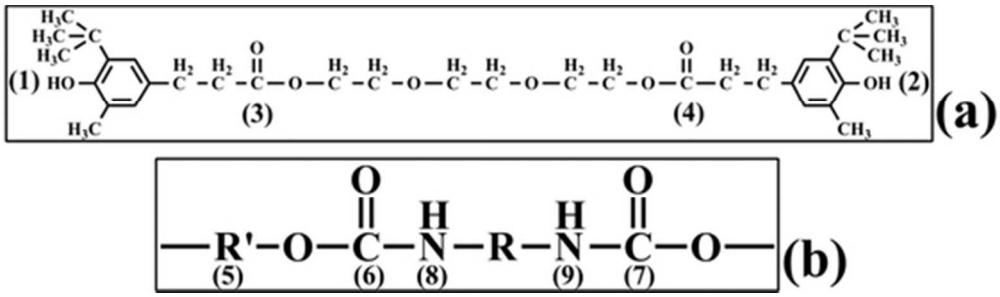

Figure 1. Molecular structures of (a) AO-70 and (b) TPU.
23x6mm (600 x 600 DPI)

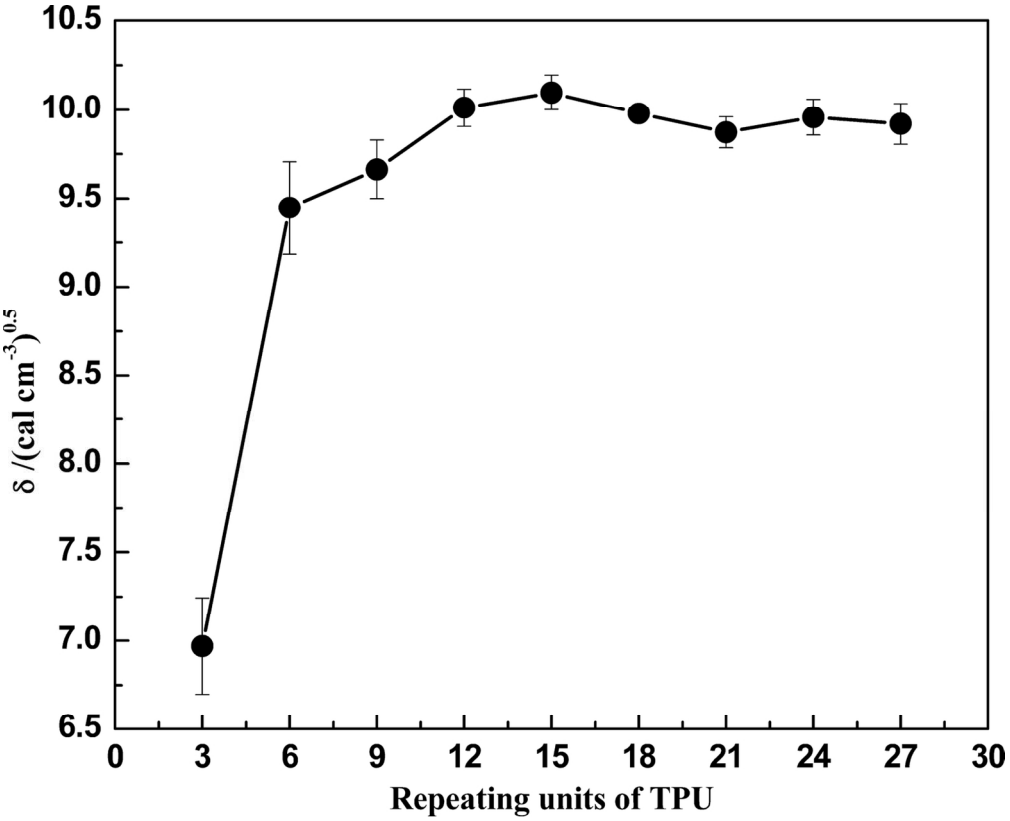

Figure 2. Solubility parameter vs repeating units of TPU.
67x54mm (600 x 600 DPI)

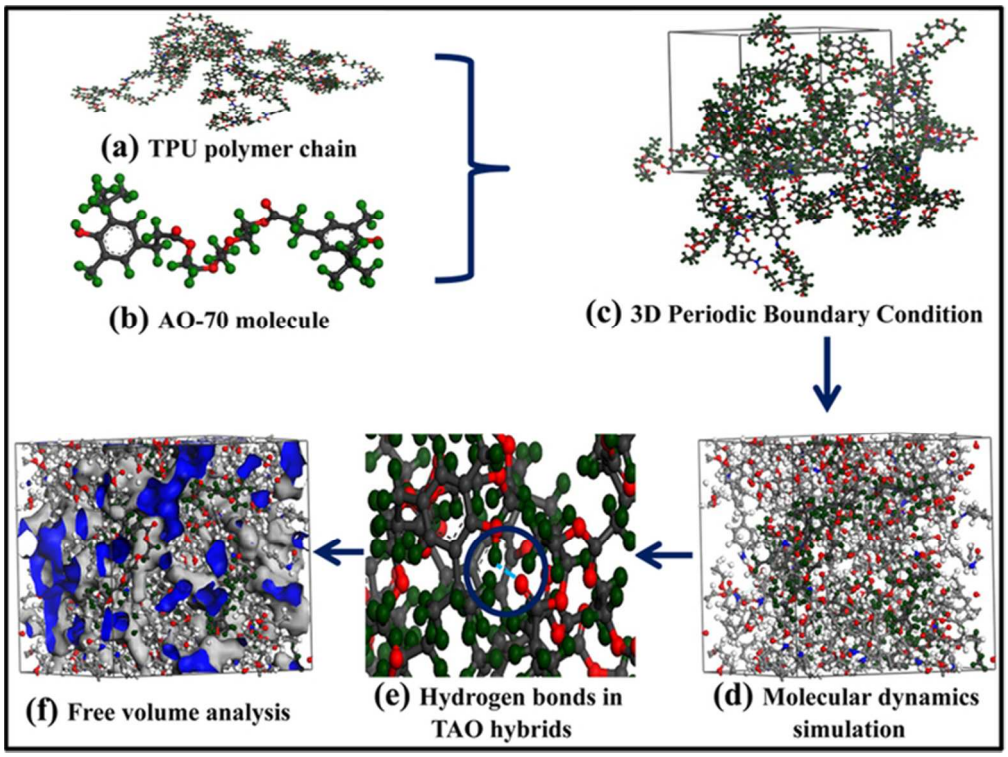

Figure 3. Models for MD simulation of TAO hybrids (red atom is O, green atom is H, grey atom is C, blue atom is N and blue dashed line represents H-bonds).
62x46mm (300 x 300 DPI)

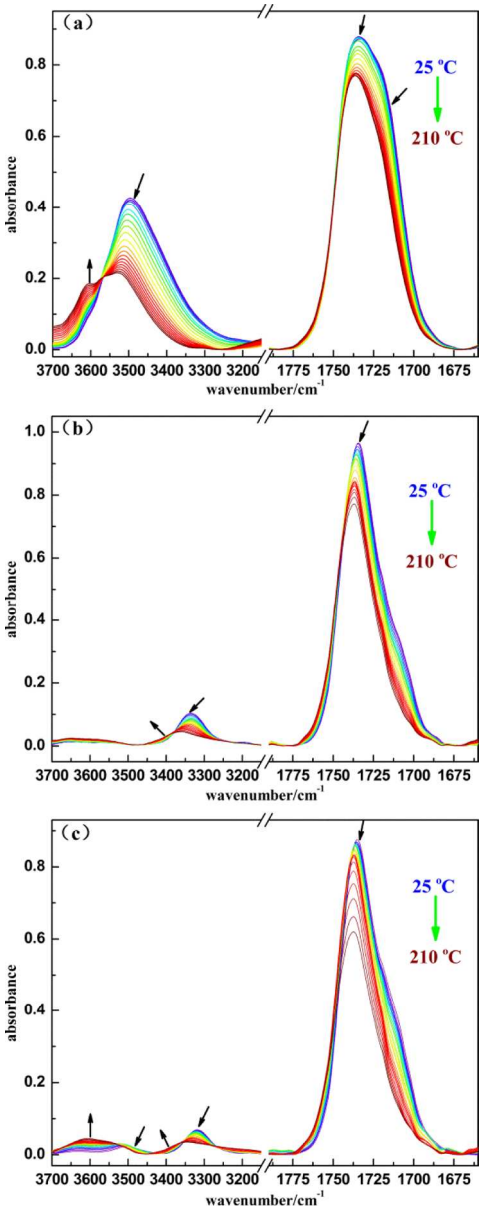

Figure 4. The temperature-dependent infrared spectrum of (a) AO-70, (b) TAO-0phr and (c) TAO-45phr in the range of 3700-3150 cm-1 and 1780-1660 cm-1 from 25 to 210°C.
210x536mm (300 x 300 DPI)

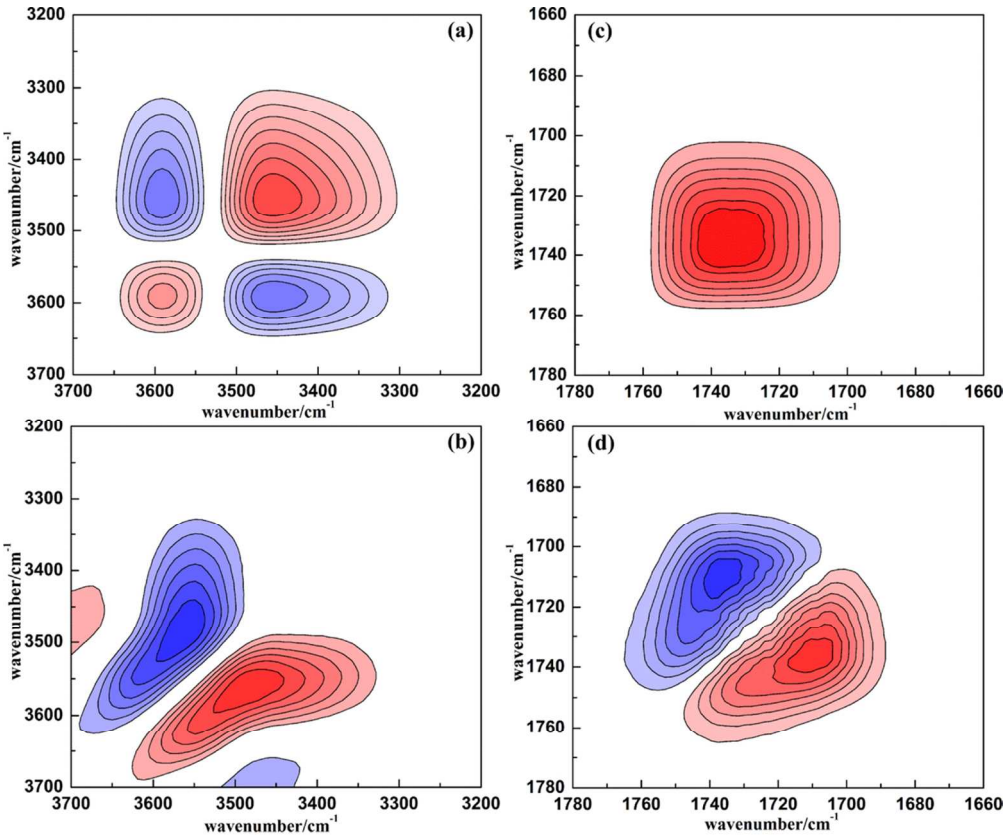

Figure 5. 2D IR correlation spectra of AO-70 obtained from 25 to 210°C: (a) synchronous map of 3700-3200 cm-1, (b) asynchronous map of 3700-3200 cm-1, (c) synchronous map of 1780-1660 cm-1, (d) asynchronous map of 1780-1660 cm-1.
115x95mm (300 x 300 DPI)

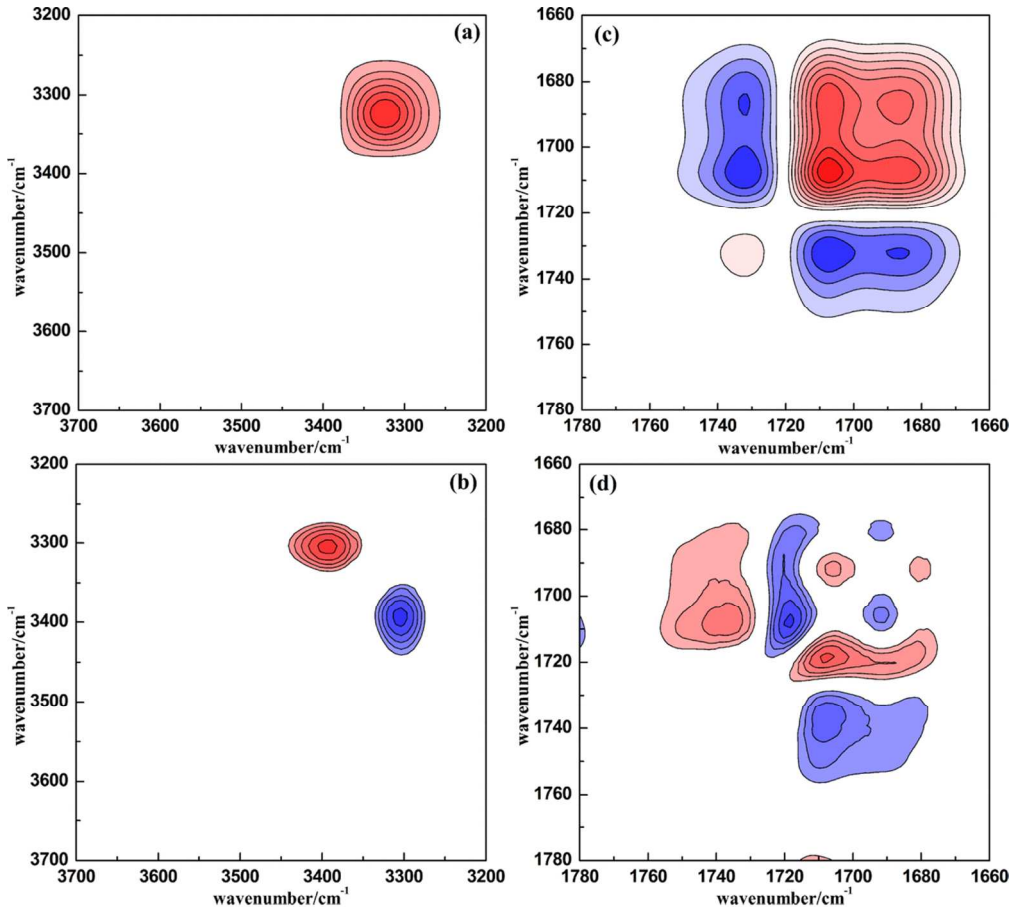

Figure 6. 2D IR correlation spectra of TAO-0phr obtained from 25 to 210°C: (a) synchronous map of 3700-3200 cm-1, (b) asynchronous map of 3700-3200 cm-1, (c) synchronous map of 1780-1660 cm-1, (d) asynchronous map of 1780-1660 cm-1.
125x112mm (300 x 300 DPI)

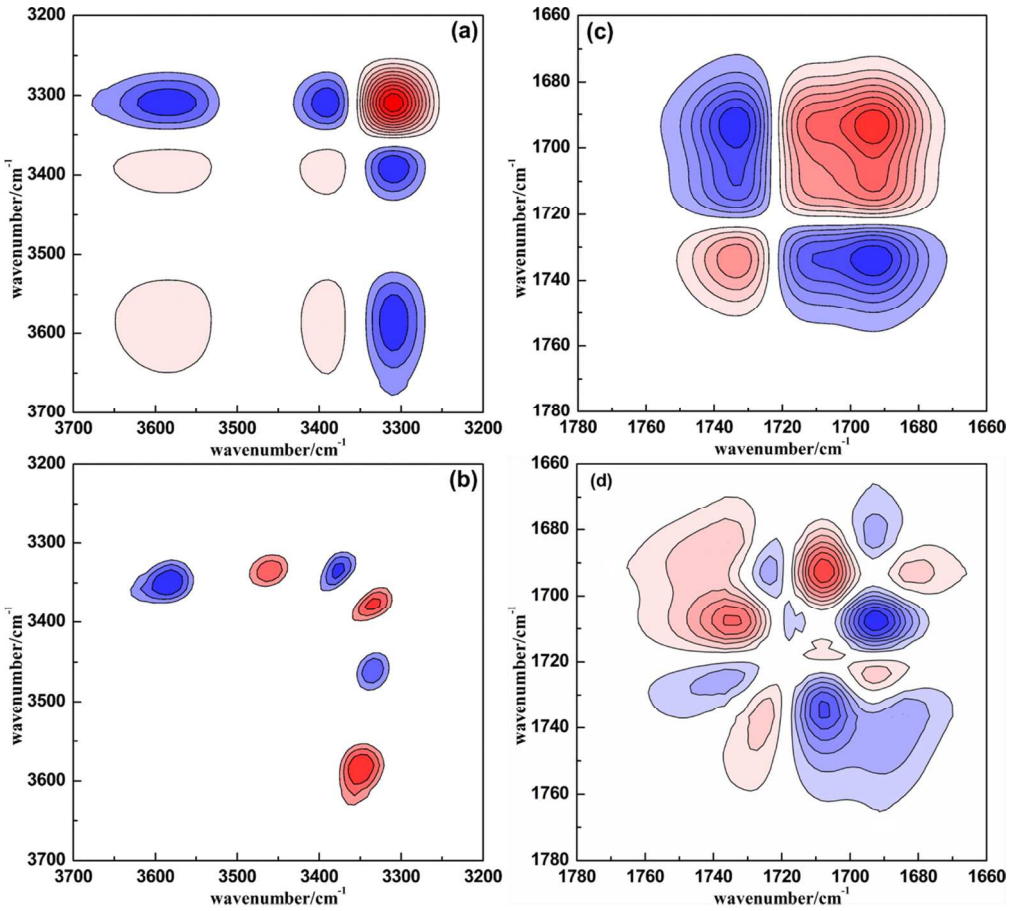

Figure 7. 2D IR correlation spectra of TAO-15phr obtained from 25 to 210°C: (a) synchronous map of 3700-3200 cm-1, (b) asynchronous map of 3700-3200 cm-1, (c) synchronous map of 1780-1660 cm-1, (d) asynchronous map of 1780-1660 cm-1.
125x113mm (300 x 300 DPI)

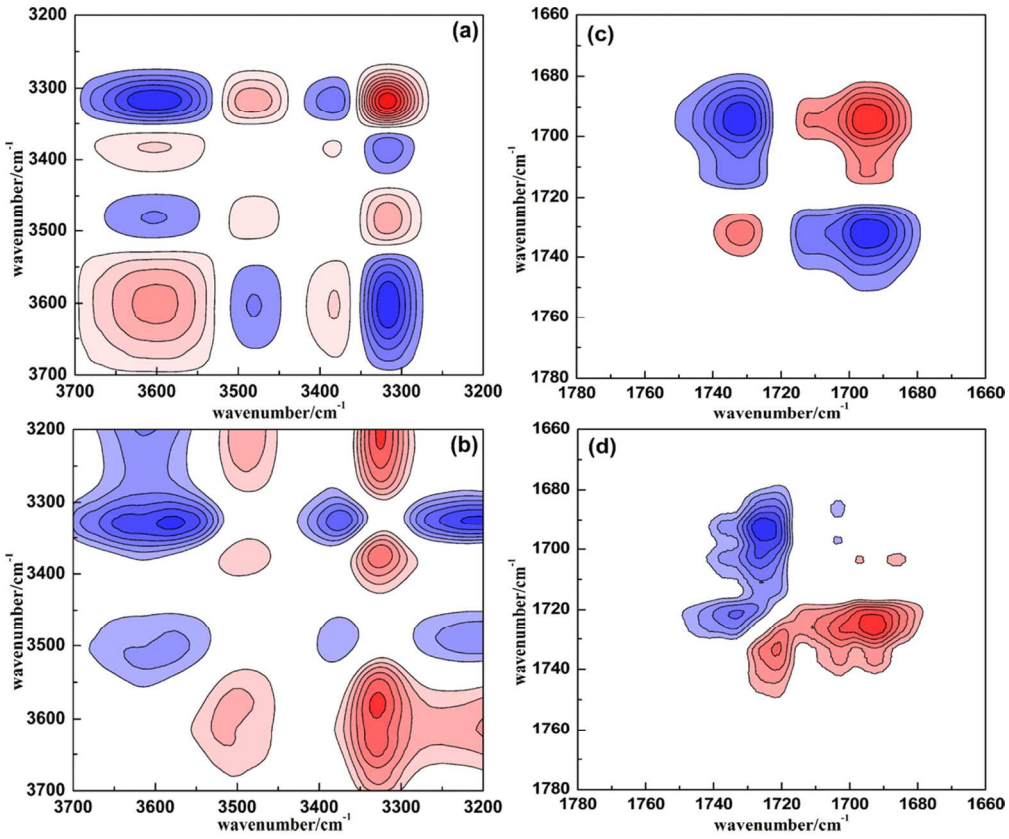

Figure 8. 2D IR correlation spectra of TAO-45phr obtained from 25 to 210°C: (a) synchronous map of 3700-3200 cm-1, (b) asynchronous map of 3700-3200 cm-1, (c) synchronous map of 1780-1660 cm-1, (d) asynchronous map of 1780-1660 cm-1.
115x95mm (300 x 300 DPI)

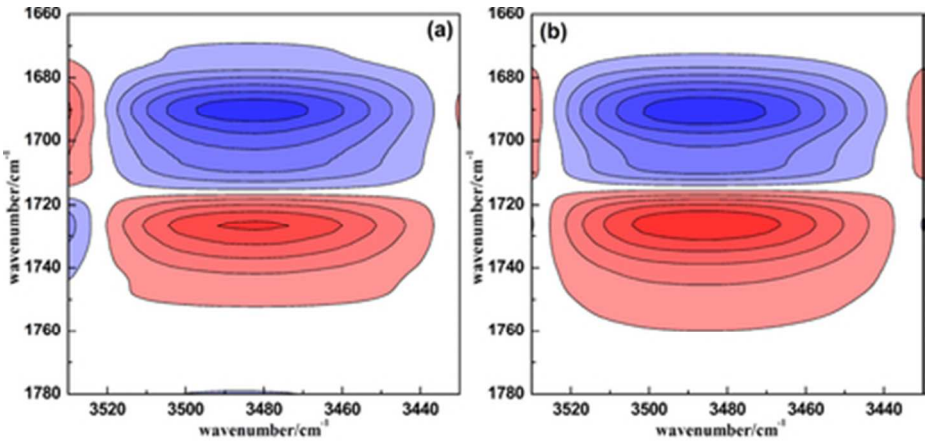

Figure 9. 2D IR correlation spectra of TAO-45phr between 3530-3430 cm-1 and 1780-1660 cm-1 regions obtained from 25 to 210°C: (a) synchronous map and (b) asynchronous map.
38x18mm (300 x 300 DPI)

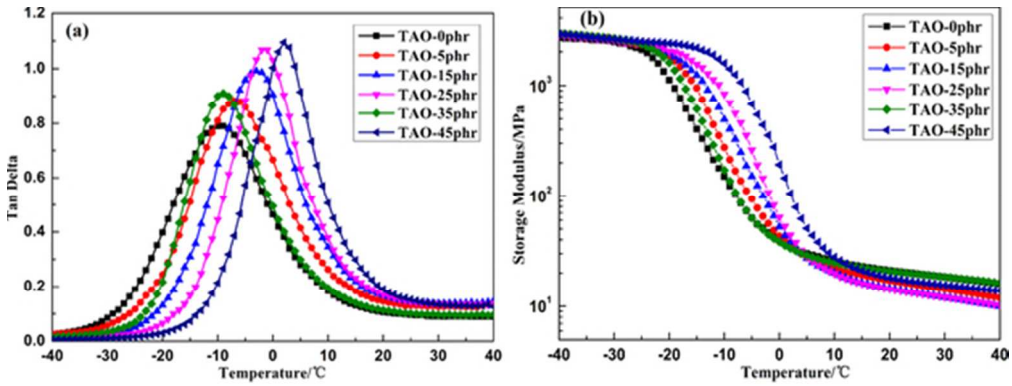

Figure 10. Temperature dependence of (a) loss factor (tanδ) and (b) storage modulus of TAO hybrids.
52x19mm (300 x 300 DPI)

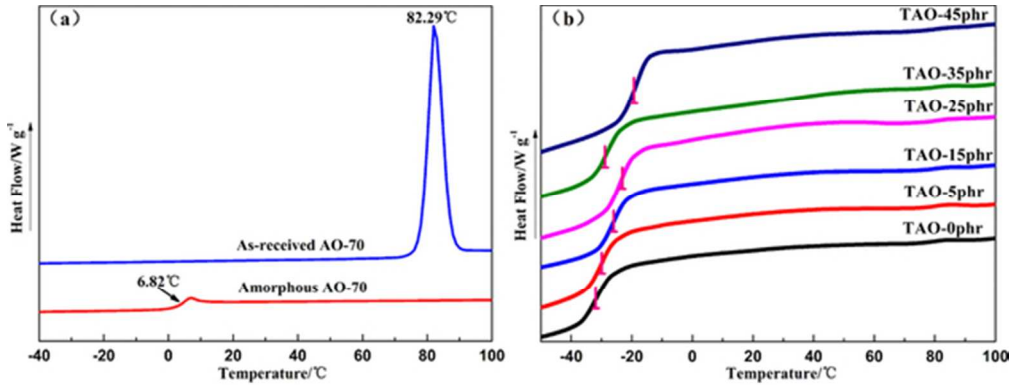

Figure 11. DSC curves of (a) AO-70 and (b) TAO hybrids.
53x20mm (300 x 300 DPI)

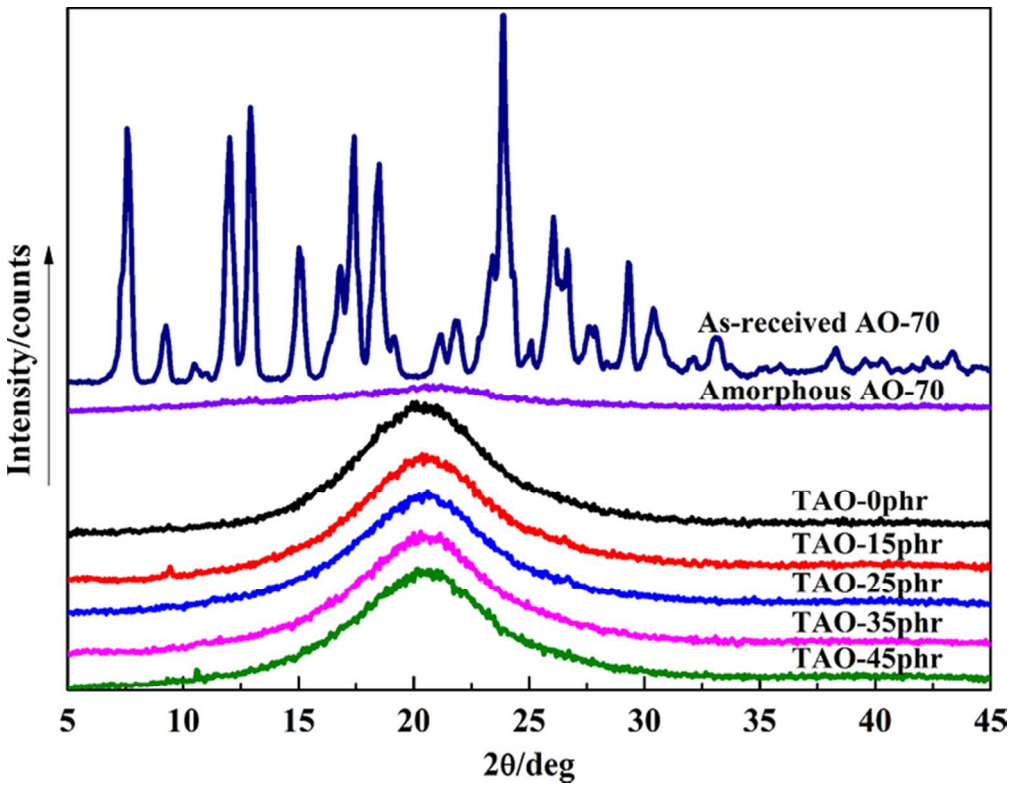

Figure 12. X-ray diffraction curves of AO-70 and TAO hybrids.
64x49mm (300 x 300 DPI)

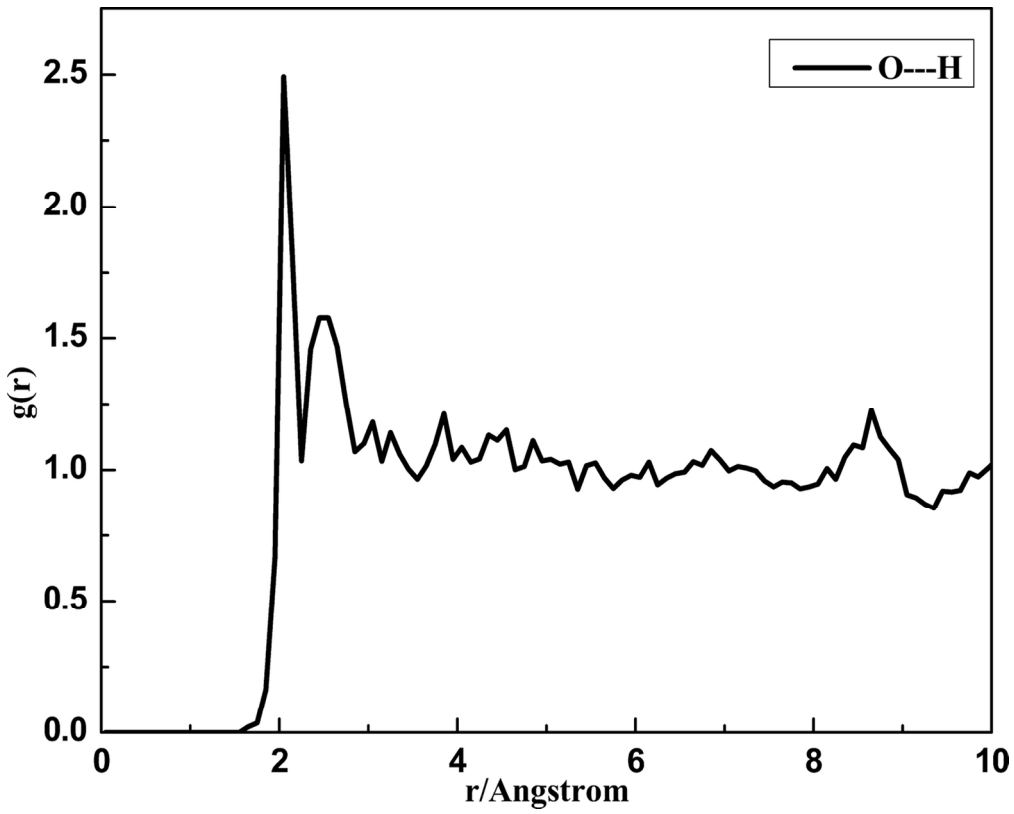

Figure 13. Pair correlation function for intermolecular H and O in TAO-25phr.
66x53mm (600 x 600 DPI)

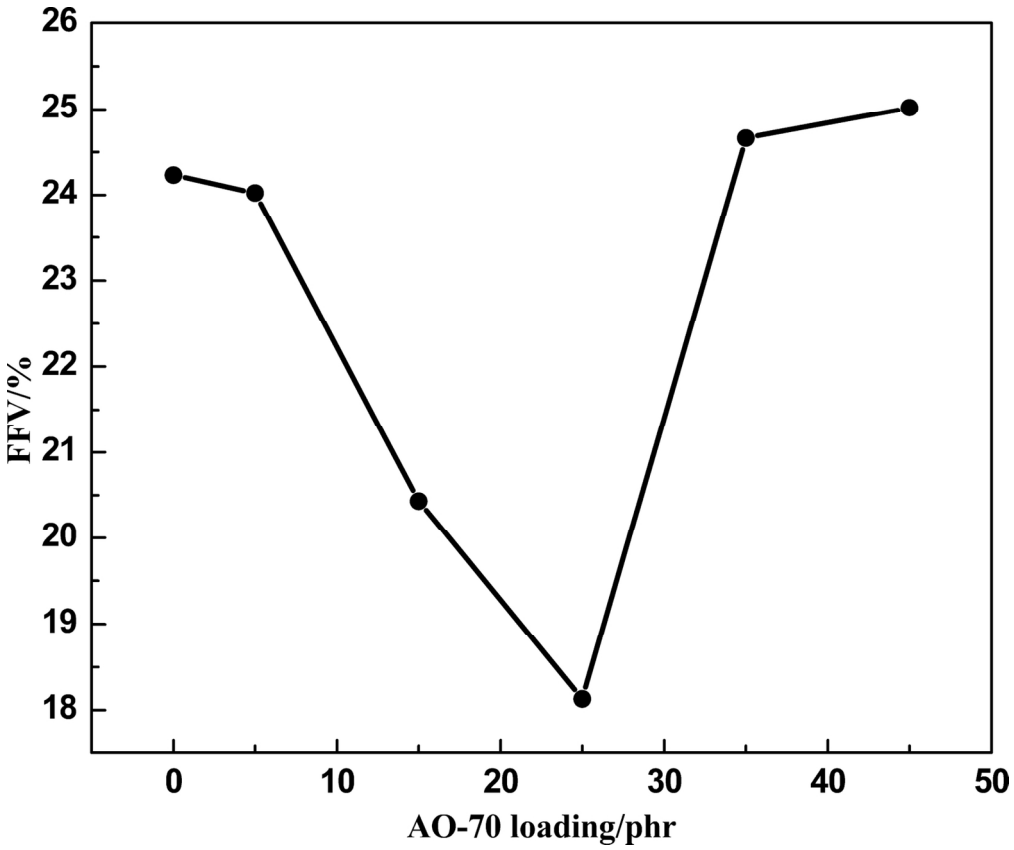

Figure 14. Fractional free volume of TAO hybrids calculated by MD simulation.
69x58mm (600 x 600 DPI)

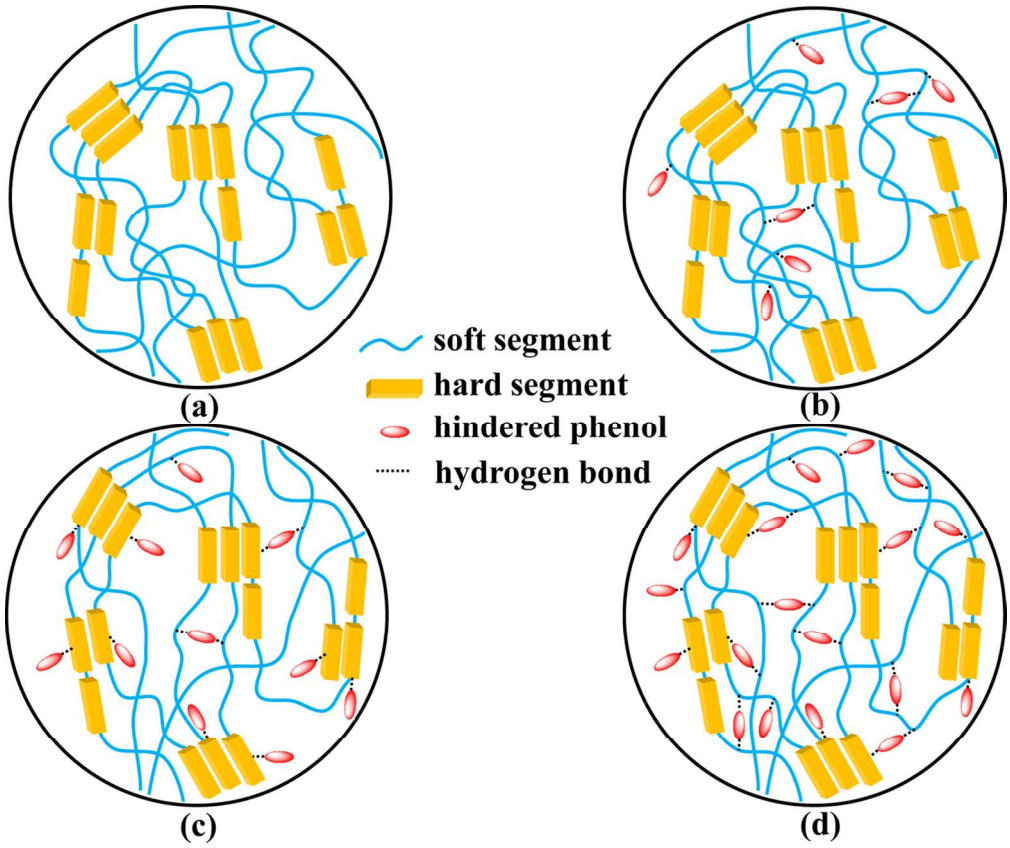

Figure 15. Structural schematic diagram represent for (a) TPU, (b) TAO-15phr, (c) TAO-35phr and (d) TAO-45phr.
117x97mm (300 x 300 DPI)

Molecular insights into hydrogen bonds in polyurethane/hindered phenol hybrids: evolution and relationship with damping properties

Kangming Xu, Fengshun Zhang, Xianlong Zhang, Qiaoman Hu, Hong Wu*, Shaoyun Guo*

State Key Laboratory of Polymer Materials Engineering, Polymer Research Institute of Sichuan University, Chengdu, Sichuan, 610065, China

*E-mail: wh@scu.edu.cn (Hong Wu); nic7702@scu.edu.cn (Shaoyun Guo).

Tel./Fax: +86-028-85406077 (Hong Wu); +86-028-85405135 (Shaoyun Guo)

Graphical abstract with text

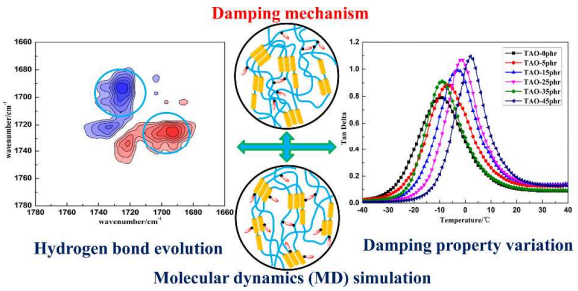

By combining experiment and MD simulation, the relationship between hydrogen bond evolution and damping property variation of TPU was revealed.